Potential of Myrtus communis Linn. as a bifunctional food: Dual high-resolution PTP1B and -glucosidase inhibition profiling combined with HPLC-HRMS and NMR for identification of antidiabetic triterpenoids and phloroglucinol derivatives

Liang, Chao; Stærk, Dan; Kongstad, Kenneth Thermann

Published in:
Journal of Functional Foods

DOI:
10.1016/j.jff.2019.103623

Publication date:
2020

Document version
Publisher's PDF, also known as Version of record

Journal of Functional Foods 64 (2020) 103623

Contents lists available at ScienceDirect

Journal of Functional Foods

journal homepage: www.elsevier.com/locate/jff

Potential of *Myrtus communis* Linn. as a bifunctional food: Dual high-resolution PTP1B and α-glucosidase inhibition profiling combined with HPLC-HRMS and NMR for identification of antidiabetic triterpenoids and phloroglucinol derivatives

Chao Liang, Dan Staerk, Kenneth T. Kongstad*

Department of Drug Design and Pharmacology, Faculty of Health and Medical Sciences, University of Copenhagen, Universitetsparken 2, DK-2100 Copenhagen, Denmark

ARTICLE INFO

Keywords:
Myrtus communis
Bifunctional food
Protein tyrosine phosphatase 1B
α-Glucosidase
Antidiabetic

ABSTRACT

Myrtus communis Linn., an aromatic shrub widely distributed in Mediterranean littoral, is traditionally used as a culinary herb and for manufacturing of the local Sardinian liquor, Mirto. In this study, the potential for developing *M. communis* into a functional food to treat type-2-diabetes (T2D) was investigated. Antidiabetic constituents in crude defatted chloroform extract of *M. communis* were pinpointed by dual high-resolution PTP1B and α-glucosidase inhibition profiling. Subsequent analytical-scale HPLC separation led to isolation and identification of 14 triterpenoids and three phloroglucinol derivatives associated with PTP1B and/or α-glucosidase inhibitory activity with IC_{50} values in the range of 8.9–69.4 μM and 34.3–88.5 μM, respectively. We also report three previously undescribed phloroglucinol derivatives. This is the first report of PTP1B inhibitors in *M. communis*, and the identification of both PTP1B and α-glucosidase inhibitors, demonstrates the potential of *M. communis* as a bifunctional food for management of T2D.

1. Introduction

Diabetes, a chronic metabolic disorder, has become one of the largest global health issues in the 21st century. According to the International Diabetes Federation, it was estimated that worldwide 425 million people were suffering from diabetes in 2017, and 4 million deaths were directly associated with diabetes (International Diabetes Federation, 2017). The cause of type 2 diabetes (T2D), which counts for 90% of all diabetes cases, is a combination of insulin resistance and an inadequate compensatory insulin secretory response (American Diabetes Association, 2013). Characterized by long-term hyperglycemia, T2D is associated with a series of severe micro- and macrovascular complications such as retinopathy, nephropathy, hypertension and microalbuminuria (Funakoshi et al., 2017; Tryggestad & Willi, 2015). Several enzymes, including α-glucosidase and protein tyrosine phosphatase 1B (PTP1B), have been proposed as clinically relevant targets for management of postprandial hyperglycemia (Huang, Yi, Yi, Bie, & Peng, 2015). α-Glucosidase, located at the epithelial mucosa of the small intestine, is a crucial digestive enzyme and a prime target for treatment of T2D. α-Glucosidase is responsible for degradation of oligosaccharides such as maltose and maltotriose into monosaccharides, which are subsequently absorbed into the blood stream (Jaiswal et al., 2012; Ibrahim, Bester, Neitz, & Gaspar, 2018). Inhibition of α-glucosidase delay the carbohydrate digestion and absorption of glucose, leading to a better management of postprandial hyperglycemia (Kazmi et al., 2018). Another promising therapeutic target is PTP1B, widely expressed in liver, muscle, brain and adipose tissues (Zabolotny et al., 2008). PTP1B functions as a negative regulator in the insulin-receptor signaling pathway by dephosphorylation of the insulin receptor, leading to a decreased insulin sensitivity or even shutdown of the signaling, further resulting in the increase of blood glucose (Johnson, Ermolieff, & Jirousek, 2002). Recently, several PTP1B inhibitors of either natural or synthetic origin have been discovered, but none are currently approved for clinical use (Bokor et al., 2017; Tamrakar,

Abbreviations: T2D, type 2 diabetes; PTP1B, protein tyrosine phosphatase 1B; *p*-NPG, *p*-nitrophenyl α-D-glucopyranoside; *p*-NPP, *p*-nitrophenyl phosphate; DMSO, dimethyl sulfoxide; Tris, tris(hydroxymethyl)-aminomethane; Bis-Tris, bis(2-hydroxyethyl)-imino-tris(hydroxymethylmethane); EDTA, *N,N,N′,N′*-ethylenediaminetetraacetate; DTT, dithiothreitol; UV, ultraviolet; HPLC, high-performance liquid chromatography; HRMS, high-resolution mass spectrometry; NMR, nuclear magnetic resonance spectroscopy

* Corresponding author.
E-mail address: kenneth.kongstad@sund.ku.dk (K.T. Kongstad).

https://doi.org/10.1016/j.jff.2019.103623
Received 23 May 2019; Received in revised form 14 September 2019; Accepted 5 October 2019
Available online 31 October 2019

Maurya, & Rai, 2014; Zhao et al., 2018). As α-glucosidase and PTP1B are two important therapeutic targets for management of T2D, discovery of α-glucosidase and PTP1B inhibitors with high selectivity and few side effects are urgently needed.

Historically, functional foods have been considered as one of the most important sources of antidiabetic drug leads. In recent years, natural products from various edible plants have been identified as inhibitors of T2D target enzymes, including α-glucosidase and PTP1B (Fang, Cao, Duan, Tang, & Zhao, 2014; Hu et al., 2017; Liu, Kongstad, Wiese, Jäger, & Staerk, 2016; Ryu et al., 2011; Xiao, Guo, Sun, & Zhao, 2017; Yue, Xu, Cao, Zhang, & Zhao, 2017). Extracts of edible plants are very complex mixtures, and identification of individual constituents responsible for the extract's observed bioactivity is a challenging task. However, this task can be aided by microplate-based high-resolution inhibition profiling, where one or more high-resolution biochromatograms are overlaid UV- or MS traces from the analytical-scale HPLC separations. This is used to pinpoint HPLC peaks correlated with bioactivity in one or more of the biochromatograms, and can thus be used to target subsequent chemical analysis towards the bioactive constituents. This technology has successfully been applied for identification of antidiabetic constituents from various edible plants (Kongstad, Özdemir, Barzak, Wubshet, & Staerk, 2015; Lima, Kato, Kongstad, & Staerk, 2018a; Schmidt, Lauridsen, Dragsted, Nielsen, & Staerk, 2012; Schmidt, Nyberg, & Staerk, 2014; Zhao, Chen, Kongstad, Jäger, & Staerk, 2017).

Myrtus communis Linn. (Myrtaceae) is an aromatic shrub widely distributed in Mediterranean littoral. Traditionally, it is used as a culinary herb and for manufacturing the local liquor, Mirto, in Sardinia, Italy (Rosa et al., 2003). Industrial use includes *M. communis* leaves as a special hop alternative in beer production and in food production for its flavouring properties (Appendino et al., 2006; Chalchat, Garry, & Michet, 1998). *Myrtus communis* has also found its use in folk medicine for treatment of various illnesses, including inflammation, bacterial infections and diabetes (Alipour, Dashti, & Hosseinzadeh, 2014; Sisay & Gashaw, 2017). The aqueous extract of *M. communis* has been reported to possess α-glucosidase inhibitory activity *in vitro* (Önal, Timur, Okutucu, & Zihnioğlu, 2005), while a 20% ethanolic extract displayed antidiabetic effect in alloxan-induced diabetic rats in vivo (Malekpour, Dehghani, Zahedi, & Eskandari, 2012). While phloroglucinol derivatives, including myrtucommulone B, C, D, and E, have been identified from *M. communis* as α-glucosidase inhibitors (Shaheen et al., 2006), no PTP1B inhibitors have previously been reported.

In this work, dual high-resolution PTP1B and α-glucosidase inhibition profiling combined with HPLC-HRMS and NMR spectroscopy were used to investigate the potential of *M. communis* as a bifunctional food to treat T2D.

2. Materials and methods

2.1. Chemicals and reagents

$NaH_2PO_4{\cdot}2H_2O$, Na_2HPO_4, NaN_3, NaOH, NaCl, *p*-nitrophenyl α-D-glucopyranoside (*p*-NPG), *p*-nitrophenyl phosphate (*p*-NPP), dimethyl sulfoxide (DMSO), α-glucosidase type I (EC 3.2.20, from *Saccharomyces cerevisiae*, lyophilized powder), tris(hydroxymethyl)-aminomethane (Tris), bis(2-hydroxyethyl)-imino-tris(hydroxymethylmethane) (Bis-Tris), *N*,*N*,*N*′,*N*′-ethylenediaminetetraacetate (EDTA), dithiothreitol (DTT), and acetic acid were purchased from Sigma-Aldrich (St. Louis, MO, USA). Recombinant human protein tyrosine phosphatase 1B (PTP1B) (BML-SE332-0050, EC 3.1.3.48) was purchased from Enzo Life Sciences (Farmingdale, NY, USA). Chloroform-*d* and methanol-d_4 were purchased from Euriso-top (Saint-Aubin Cesex, France) and formic acid from Merck (Darmstadt, Germany). HPLC-grade acetonitrile, methanol, chloroform and petroleum ether (b.p. 40–65 °C) were purchased from Sigma-Aldrich (St. Louis, MO, USA). Water was prepared by filtration and deionization on a Milli-Q Plus system through a 0.22-μm membrane filtration system (Millipore, Billerica, MA, USA).

2.2. Plant material, extraction and sample preparation

The leaves of *M. communis* Linn. were collected in Isfahan, Iran in 1999. A voucher specimen (No. 9055) was deposited in the herbarium of the Isfahan Research Centre of Natural Resources and Animal Science (Isfahan, Iran). The air-dried and powdered leaves of *M. communis* (30 g) was extracted with 600 mL chloroform (3 × 200 mL) by ultrasonication for 2 h. The extract was filtered through Whatman filter paper and lyophilized on a rotary evaporator before being redissolved in 400 mL 90% methanol and defatted with 300 mL petroleum ether (b.p. 40–65 °C) in a separation funnel. The methanolic phase was evaporated to dryness on a rotary evaporator to yield 560 mg defatted chloroform extract.

2.3. PTP1B inhibitory assay

The PTP1B inhibitory assay was performed in 96-well microplates as previously described (Wubshet et al., 2016). In brief, the material in all wells were dissolved in 18 μL DMSO followed by addition of 52 μL EDTA solution (3.46 mM in a buffer consisting of 50 mM Tris, 50 mM Bis-Tris and 0.1 M NaCl, adjusted to pH 7.0 with acetic acid), and 60 μL substrate solution containing 1.5 mM *p*-NPP, and 6 mM DTT in the aforementioned buffer. The microplates were incubated at 25 °C for 10 min before adding 50 μL of a 1.0 μg/mL PTP1B stock solution to initiate the enzymatic reaction. The absorbance of each well was measured at 405 nm every 30 s for 10 min to yield the enzyme activity (cleavage rate) expressed as ΔAU/min. Incubation and measurement of absorbance were conducted with a Thermo Scientific Multiskan FC microplate photometer (Thermo Scientific, Waltham, MA, USA) with a built-in incubator controlled by SkanIt ver. 2.5.1 software. All measurements were performed in triplicate with pure DMSO used as blank sample and RK-682 as reference compound. The enzyme inhibition was calculated using the following equation:

$$\text{Percentage inhibition} = [(\text{Slope}_{\text{blank}} - \text{Slope}_{\text{sample}})/\text{Slope}_{\text{blank}}] \times 100\%$$

2.4. α-Glucosidase inhibitory assay

The α-glucosidase inhibitory assay was performed in 96-well microplates as previously described (Zhao, Kongstad, Jäger, Nielsen, & Staerk, 2018). Briefly, samples were dissolved in 10 μL DMSO followed by addition of 90 μL phosphate buffer (100 mM containing 34 mM $NaH_2PO_4{\cdot}2H_2O$, 66 mM Na_2HPO_4 and 0.02% NaN_3, adjusted to pH 7.5 with NaOH), whereafter the microplates were shaken for 10 min. After mixing, 80 μL α-glucosidase enzyme solution (2.0 U/mL), prepared with the aforementioned phosphate buffer, was added to each well and the microplates were incubated at 28 °C for additional 10 min. The enzymatic reaction was initiated by adding 20 μL *p*-NPG solution (10 mM in phosphate buffer), and the absorbance of the cleavage product, *p*-nitrophenol, was then measured at 405 nm every 30 s for 35 min, to yield the enzyme activity expressed as ΔAU/s. Incubation and measurement of absorbance were conducted with the Thermo Scientific Multiskan FC microplate photometer described above. All measurements were performed in triplicate with pure DMSO used as blank and acarbose as reference compound. The enzyme inhibition was calculated using the same equation as for the PTP1B assay.

2.5. Microfractionation and high-resolution PTP1B/α-glucosidase inhibition profiling

Analytical-scale chromatographic separations were performed on an Agilent 1200 series instrument (Santa Clara, CA, USA) consisting of a

G1367C high-performance autosampler, a G1311A quaternary pump, a G1322A degasser, a G1316A thermostatted column compartment, a G1315C photodiode array detector, and a G1364C fraction collector, all controlled by Agilent ChemStation version B.03.02 software.

The crude extract was separated on a reversed-phase Phenomenex Luna C_{18}(2) column (150 × 4.6 mm i.d., 3 µm particle size, 100 Å pore size; Phenomenex, Torrance, CA, USA), whereas the chromatographic peaks *2*, *5*, *11*, and *13* were further separated and microfractionated on a Phenomenex Kinetex PFP column (150 × 4.6 mm i.d., 2.6 µm particle size, 100 Å pore size). The solvent system for the C_{18} column consisted of a mixture of acetonitrile-water (5:95, v/v; solvent A) and acetonitrile-water (95:5, v/v; solvent B), whereas for the PFP column acetonitrile was exchanged by methanol. All solvents were acidified with 0.1% formic acid. The flow rate was 0.5 mL/min and the temperature of both columns was maintained at 40 °C.

For PTP1B and α-glucosidase inhibition profiling of the crude chloroform extract, two injections of 20 µL (20 mg/mL in methanol) were separated using the following gradient: 0 min, 50% B; 30 min, 100% B; 40 min, 100% B; 42 min, 50 %B. For each injection, the eluent from 5 to 40 min was fractionated into 88 wells of a 96-well microplate, leading to a resolution of 2.51 data points/min.

For peaks *2* and *5*, a 10 µL injection of each (of 9 mg/mL and 8 mg/mL methanol solution, respectively) was separated on the PFP column using the following gradient: 0 min, 70% B; 30 min, 100% B; 40 min, 100% B; 42 min, 70% B. The eluent from 3 to 22 min was fractionated into 44 wells of a 96-well microplate, leading to a resolution of 2.32 data points/min. For peak *11*, a 3 µL injection (of a 9 mg/mL methanol solution) was separated using the following elution gradient: 0 min, 70% B; 10 min, 80% B; 30 min, 80% B; 40 min, 100% B; 48 min, 100% B; 50 min, 70% B. The eluent from 20 to 32 min was fractionated into 40 wells of one 96-well microplate, leading to a resolution of 3.33 data points/min. For peak *13*, a 10 µL injection (10 mg/mL in methanol) was separated using the following elution gradient: 0 min, 70% B; 30 min, 100% B; 40 min, 100% B; 42 min, 70% B. The eluent from 17 to 21 min was fractionated into 10 wells of one 96-well microplate, leading to a resolution of 2.75 data points/min. All microplates were subsequently evaporated to dryness using a Savant SPD121P speed vacuum concentrator equipped with an OFP400 oil-free pump and an RVT400 refrigerated vapor trap (Holbrook, NY, USA). The microfractionated crude extract was investigated for α-glucosidase inhibitory activities, while both the crude extract and the fractionated peaks *2*, *5*, *11*, and *13* were investigated for PTP1B inhibitory activities. High-resolution PTP1B and α-glucosidase biochromatogram were produced by plotting the percent inhibition of each well against the corresponding retention time of the HPLC chromatogram.

2.6. Determination of IC_{50} values of crude extract and active compounds towards PTP1B and α-glucosidase

Dose-dependent effect of the defatted chloroform extract of *M. communis* and compounds showing PTP1B and/or α-glucosidase inhibitory activity were determined using the protocol described above, with the exception that 10 µL of two-fold serial dilutions of analytes and reference compounds were added to each well in triplicate. Calculation of IC_{50} values and generation of dose-response curves (Supplementary material) were done in GraFit software, version 5.0.11 (Erithacus Software Limited) using the following function:

$$f(x) = \min + \frac{\max - min}{1 + \left(\frac{x}{IC_{50}}\right)^{slope}}$$

where min is the background, max – min is the y-range, x is the concentration and slope is the Hill slope. Results are reported as IC_{50} values ± standard error.

2.7. Determination of mode of inhibition

Detailed kinetic studies of PTP1B inhibition for **1**, **3**, **4**, **6**, **8**, **9** and **10** were performed to determine their mode of inhibition, using the standard assay conditions described in Section 2.3. Three concentrations of *p*-NPP (0.5, 1 and 2 mM) combined with different concentrations of the investigated compounds were assayed to measure the kinetic rate expressed as ΔAU/min. Detailed kinetic studies of α-glucosidase inhibition for **8**, **9** and **10** were performed to determine their mode of inhibition using the standard assay conditions described in Section 2.4. Five concentrations of *p*-NPG (0.1875, 0.375, 0.75, 1.5 and 3 mM) combined with different concentrations of the investigated inhibitors were assayed to measure the kinetic rate expressed as ΔAU/min. All measurements were performed in triplicate. Kinetic parameters were calculated by fitting the data to the Michaelis-Menten equation using non-linear regression analysis (GraphPad Prism version 8.1.2, GraphPad Software, Inc.). The mode of inhibition was determined by Lineweaver-Burk plot analysis (GraphPad Prism version 8.1.2).

2.8. Analytical scale isolation

Forty successive injections of crude defatted chloroform extract of *M. communis* (25 µL of 50 mg/mL in methanol) were separated using a reversed-phase Phenomenex Luna C_{18} (2) column (150 × 4.6 mm i.d., 3 µm particle size, 100 Å pore size) for accumulation of compounds **1** (1.38 mg), **3** (0.50 mg), **4** (0.50 mg), **6** (0.63 mg), **7** (1.58 mg), **8** (1.25 mg), **9** (1.09 mg), **10** (1.68 mg), **12** (0.69 mg), **14** (0.80 mg), and **15** (0.40 mg) by automatic fraction collection using the same method and equipment as for the microfractionation. In addition to the isolated compounds, peaks *2* (1.38 mg), *5* (1.43 mg), *11* (2.00 mg), and *13* (1.24 mg) were isolated for further purification as follows.

Fifteen successive injections (10 µL of a 9 mg/mL methanol solution) of peak *2*, eighteen successive injections (10 µL of a 8 mg/mL methanol solution) of peak *5*, twenty-seven successive injections (8 µL of a 9 mg/mL methanol solution) of peak *11* (see Supplementary Fig. S26) and twenty-five successive injections (5 µL of a 10 mg/mL methanol solution) of peak *13* were separated according to the method used for the microfractionation. Exceptions were peak *2* and *5*, which were separated using the following gradients, respectively: 0 min, 60% B; 25 min, 75% B; 30 min, 100% B; 38 min, 100% B; 40 min, 60% B, and 0 min, 65% B; 30 min, 82% B; 40 min, 100% B; 48 min, 100% B; 50 min, 65% B, using the Phenomenex PFP column.

The isolation procedures led to accumulation of compounds **2a** (0.20 mg), **2b** (0.02 mg), **2c** (0.02 mg), **5a** (0.20 mg), **5b** (0.15 mg), **11b** (0.13 mg), and **13c** (0.56 mg) together with peak *11a* (0.30 mg) by automatic fraction collection based on thresholds at 210 nm for **2a**, **5a** and **5b**, 254 nm for **2b** and **2c**, and 310 nm for peak *11a* and compound **11b**.

Peak *11a* (see Supplementary Fig. S27) was further purified on a Phenomenex Luna C_{18}(2) column (150 × 4.6 mm i.d., 3 µm particle size, 100 Å pore size) using the following elution gradient: 0 min, 85% B; 10 min, 100% B; 15 min, 100% B; 17 min, 85 %B. This led to isolation of compounds **11a-1** (0.15 mg) and **11a-2** (0.05 mg), collected by automatic fraction collection using a threshold at 254 nm.

2.9. HPLC-HRMS experiments

Molecular formulas of isolated compounds were obtained through analysis on an Agilent 1260 HPLC system consisting of a G1311B quaternary pump with a built-in degasser, a G1329B autosampler, a G1316A thermostatted column compartment, and a G1315D photodiode array detector, coupled with a Bruker micrOTOF-Q II mass spectrometer (Bruker Daltonik, Bremen, Germany) equipped with the ESI source. Mass spectra were acquired in negative-ion mode with a capillary voltage of 3500 V and positive mode at 4100 V, a drying temperature of 200 °C, a nebulizer pressure of 2.0 bar and a drying gas

flow of 7 L/min. A solution of sodium formate clusters was automatically injected at the beginning of the analysis to enable internal mass calibration. Chromatographic separation was obtained using the same methods and conditions as for the microfractionation of the crude chloroform extract as well as peaks *2*, *5*, *11*, *13*, and *11a*.

2.10. NMR experiments

All NMR experiments were performed on a Bruker Avance III system (^{1}H operating frequency of 600.13 MHz, ^{13}C 150.90 MHz) equipped with a Bruker SampleJet sample changer and a cryogenically cooled gradient inverse triple-resonance 1.7 mm TCI probe-head (Bruker Biospin, Karlsruhe, Germany) at 300 K. NMR data were acquired in methanol-d_4, except for **8**, **9** and **10**, which were acquired in chloroform-*d*. The residual solvent signals were used for calibration of ^{1}H and ^{13}C chemical shifts for both methanol-d_4 (δ_H 3.31 ppm and δ_C 49.00 ppm) and chloroform-*d* (δ_H 7.26 ppm and δ_C 77.16 ppm). ^{1}H spectra were acquired using 30° pulses, a spectral width of 20 ppm, acquisition time of 2.72 s, relaxation delay of 1.0 s, and 64 k data points; whereas ^{13}C spectra were acquired with 30° pulses with spectral width 240 ppm, acquisition time 0.90 s and relaxation delay 2.0 s and 64 k data points. DQF-COSY and ROESY spectra were acquired using a gradient-based pulse sequence with spectral width 20 ppm and 2 k × 512 data points (processed with forward linear prediction to 1 k data points). HSQC spectra were acquired with spectral width 12 ppm for ^{1}H and 170 ppm for ^{13}C, 2 k × 256 data points (processed with forward linear prediction to 1 k data points), and relaxation delay 1.0 s. HMBC spectra were acquired with spectral width 12 ppm for ^{1}H and 240 ppm for ^{13}C, 2 k × 128 data points (processed with forward linear prediction to 1 k data points), and relaxation delay 1.0 s. Icon NMR (version 4.2, Bruker Biospin, Karlsruhe, Germany) was used for controlling automated acquisition of NMR data, and NMR data were processed by using Topspin (version 3.5, Bruker Biospin).

3. Results and discussion

Crude defatted chloroform extract of *M. communis* displayed potent PTP1B inhibition with an IC_{50} value of 9.36 μg/mL and moderate α-glucosidase inhibition with an IC_{50} value of 22.33 μg/mL. The extract was therefore subjected to dual high-resolution PTP1B and α-glucosidase inhibition profiling with the aim of pinpointing all constituents correlated with PTP1B and/or α-glucosidase inhibitory activity.

3.1. Dual high-resolution PTP1B and α-glucosidase inhibition profiling of crude defatted chloroform extract

The HPLC eluate from 5 to 40 min was fractionated into 88 wells of one 96-well microplate. After two consecutive separations on individual 96-well microplates, following evaporation of the HPLC eluate, the two plates were subjected to PTP1B and α-glucosidase assaying, respectively. The results expressed as percent inhibition were plotted at their corresponding retention times to provide a dual high-resolution biochromatogram with a resolution of 2.51 data points/min (Fig. 1). The dual high-resolution biochromatogram showed that peaks *1–5* were only correlated with PTP1B inhibitory activity, whereas peaks *6–15* were correlated with both α-glucosidase and PTP1B inhibitory activity.

3.2. High-resolution PTP1B inhibition profiling of peaks 2, 5, 11 and 13

HPLC-HRMS analysis of the material collected as peaks *2*, *5*, *11* and *13* indicated that they consisted of a mixture of compounds. They were therefore microfractionated after analytical-scale HPLC separation on a PFP column, whereafter high-resolution PTP1B inhibition profiles were prepared. This allowed pinpointing of PTP1B inhibitory constituents in peaks *2*, *5*, and *13* (see inserts in Fig. 1), whereas the results from the biochromatogram of peak *11* didn't allow direct pinpointing of PTP1B inhibitors, and all major metabolites in this fractions were therefore isolated.

3.3. Identification and pharmacological characterization of active triterpenoids

Fourteen active triterpenoids were identified by comparison of HRMS data as well as 1D and 2D NMR data with data from literature. According to the high resolution biochromatograms (Fig. 1), arjunolic acid (**1**) (Zebiri et al., 2017), asiatic acid (**2a**) (Aguirre et al., 2006), 3β-*cis-p*-coumaroyloxy-2α,23-dihydroxyolean-12-en-28-oic acid (**3**) (Gu et al., 2001), 3β-*trans-p*-coumaroyloxy-2α,24-dihydroxy-urs-12-en-28-oic acid (**4**) (Sashida et al., 1994), 23-hydroxyursolic acid (**5a**) (Wang, Xiang, Chen, Zhang, & He, 2012), hederagenin (**5b**) (Seitimova, Eskalieva, Burasheva, & Choudhary, 2018), 3β-*O-cis-p*-coumaroyl-2α-hydroxy-urs-12-en-28-oic acid (**11a-1**) (Häberlein & Tschiersch, 1994), and 3β-*O-trans-p*-coumaroyl maslinic acid (**11b**) (Lima et al., 2018b) were correlated with PTP1B inhibitory activity, whereas maslinic acid (**6**) (Lima et al., 2018b), corosolic acid (**7**) (Aguirre et al., 2006), jacoumaric acid (**12**) (Lee, Juang, Hsu, & Wu, 2005), betulinic acid (**13c**) (Eyong et al., 2018), oleanolic acid (**14**) (Martinez et al., 2013), and ursolic acid (**15**) (Lima et al., 2018b) were correlated with both PTP1B and α-glucosidase inhibitory activity. Dose response curves (Supplementary Fig. S1) of the isolated triterpenoids revealed compounds **3**, **4**, **6**, **7**, **11a-1**, **12**, **13c**, **14**, and **15** to exhibit potent PTP1B inhibitory activity with IC_{50} values below 30 μM (Table 1) with this being the first report of PTP1B inhibitory activity of **3**, **4**, **11a-1** and **12**. Compounds **1**, **5a**, and **11b** showed moderate PTP1B inhibitory activity with IC_{50} values ranging from 34.82 to 69.39 μM. Compound **5b** was not tested due to limited amount of material but has previously been reported to possess a PTP1B inhibitory activity of 9.53 μM (Zhao, Kongstad, Liu, He, & Staerk, 2019). Dose response curves (Supplementary Fig. S2) revealed **7**, **14** and **15** as moderate α-glucosidase inhibitors with IC_{50} values ranging from 34.29 to 62.27 μM. Due to limited amounts of **2a**, determination of IC_{50} value of this was unsuccessful.

The active triterpenoids of sufficient amounts (**1**, **3**, **4**, and **6**) were analysed for their mode of inhibition showing mixed-mode PTP1B inhibition for compounds **1**, **3**, and **4** while compound **6** is a competitive PTP1B inhibitor (see supplementary Fig S28).

3.4. Identification and pharmacological characterization of active phloroglucinol derivatives

Investigation of the high-resolution biochromatograms and HPLC-HRMS data indicated that HPLC peaks *8–10* were three phloroglucinol derivatives, correlating with both PTP1B and α-glucosidase inhibitory activity, namely myrtucommulone B (**8**) (Wiechmann et al., 2015), 5,7-dihydroxy-6-isobutyryl-2,2,10,10,12,12-hexamethyl-2,3,3a,4-tetrahydro-4,9a-propanofuro[2,3-b]chromen-11-one (**9**) (Liu et al., 2017), and isomyrtucommulone B (**10**) (Appendino et al., 2002). While both **8** and **10** have previously been isolated from *M. communis*, this is the first report of **9**, having the uncommon tetracyclic ketal skeleton, being isolated from nature. Compound **9** has previously been identified as an intermediate in the total synthesis of myrtucommulone J (Liu et al., 2017).

As seen in Table 1, IC_{50} values towards PTP1B were 39.71, 39.66, and 8.93 μM for **8**, **9**, and **10**, respectively, with mixed mode inhibition profiles for **8** and **9**. While the curve for **10** was inconclusive, it is reasonable to assume mixed mode inhibition for this as well (Fig. S28). IC_{50} values towards α-glucosidase were 88.54, 85.79, and 71.77 μM with non-competitive inhibition profiles (Fig. S29) Interestingly, with an IC_{50} value of 8.93 μM, similar to the reference compound, RK-682, **10** exhibited nearly 4.5-fold stronger PTP1B inhibitory activity compared to the regioisomer **8**. In a previous study, **8** was found to possess α-glucosidase inhibitory activity (Shaheen et al., 2006), but this is the

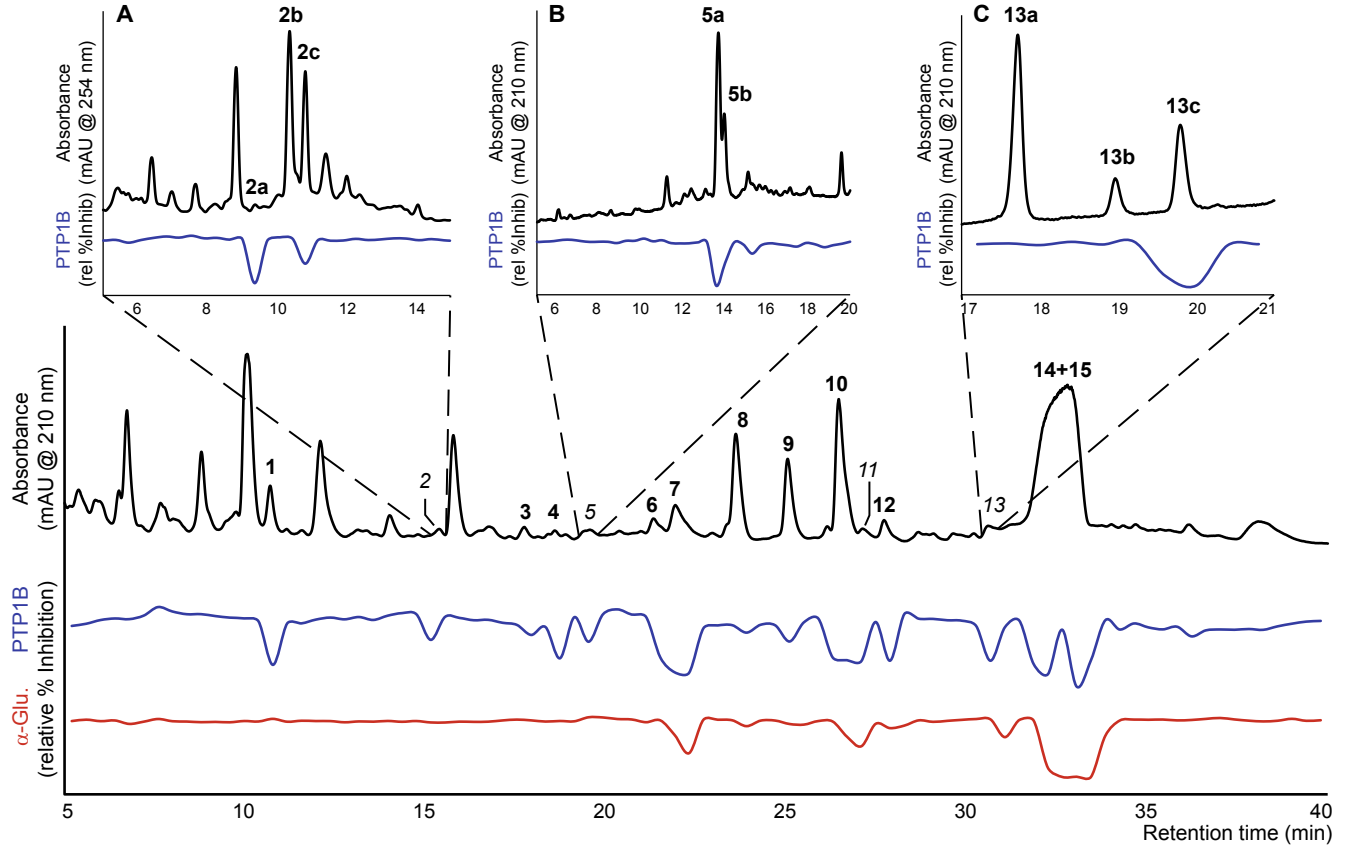

Fig. 1. HPLC chromatogram at 210 nm overlaid with dual-high resolution PTP1B and α-glucosidase inhibition profiles of crude defatted chloroform leaves extract of *Myrtus communis*; **A.** HPLC chromatogram at 254 nm overlaid with high resolution PTP1B inhibition profile of peak *2*; **B.** HPLC chromatogram at 210 nm overlaid with high resolution PTP1B inhibition profile of peak *5*; **C.** HPLC chromatogram at 210 nm overlaid with high resolution PTP1B inhibition profile of peak *13*.

first report of α-glucosidase inhibitory activity of **9** and **10** as well as PTP1B inhibitory activity of compounds **8–10**.

Phloroglucinol derivatives, such as compounds **8–10**, containing variations of a tetramethylcyclohexenedione moiety, have exclusively been found in the Myrtaceae family. The combination of uncommon carbon skeletons and a broad range of bioactivities, including antibacterial, anticancer, antiviral, and anti-inflammatory activity (Chen et al., 2017; Choudhary et al., 2013; Liu et al., 2016), has sparked an interest in semi- and total synthesis of these compounds in recent years (Liu et al., 2017; Lv, Li, Zhang, & Xie, 2017). The findings presented here, further emphasize the potential of developing *M. communis* into a bifunctional (as evidenced by the findings in this paper) or polyfunctional food (as interpreted from the other bioactivities reported for phloroglucinols) with health-promoting effect against a variety of diseases due to this specialization into producing structurally unique phloroglucinol derivatives.

3.5. Identification of new phloroglucinol derivatives

While compound **2b** did not correlate with PTP1B or α-glucosidase inhibitory activities in the high-resolution biochromatogram, similarities in UV spectra and identical molecular formulas between **2b** and the active compound **2c** (see Supplementary Fig. S25), it was speculated that these were isomers. Compound **2b** was thus also targeted for structural identification. Due to limited amounts of **2c**, determination of its IC_{50} value was unsuccessful.

Compound **2b** was obtained as a white gum. The assignment of its molecular formula as $C_{24}H_{38}O_5$ was based on the quasi-molecular ion observed in the HRESI(+)MS spectrum at *m/z* 407.2792 $[M + H]^+$ (calcd for $C_{24}H_{39}O_5^+$ 407.2792, ΔM 0.0 ppm). The ^{1}H NMR spectrum of **2b** indicated the presence of one oxymethine proton at δ_H 3.50 ppm (brs, H-3′), two methyl doublets at δ_H 0.96 ppm (J = 6.8 Hz, CH_3-9) and 0.64 ppm (J = 6.8 Hz, CH_3-10), and six methyl singlets at δ_H 1.41 ppm (CH_3-14), 1.39 ppm (CH_3-13), 1.32 ppm (CH_3-9′), 1.31 ppm (CH_3-11), 1.26 ppm (CH_3-12) and 1.16 ppm (CH_3-7′) (Table 2). ^{13}C NMR chemical shift obtained from HSQC and HMBC spectra indicated the presence of 24 carbons including eight methyl carbons at δ_C 27.5 ppm, 26.6 ppm, 25.5 ppm, 25.2 ppm, 24.6 ppm, 22.5 ppm, 20.7 ppm, 15.7 ppm, two carbonyl carbons at δ_C 214.7 ppm and 199.4 ppm, two olefinic carbons at δ_C 173.0 ppm, and 112.8 ppm, and three oxygenated carbons at δ_C 83.5 ppm, 73.9 ppm, and 71.6 ppm (Table 2). Comparison of the NMR data with those of the known isomers myrtucomvalones A and B, indicated the presence of an isobutyl syncarpic acid moiety (Chen et al., 2017). This was furthermore supported by HMBC correlations from H-11 and H-12 to C-1, C-2, and C-3, from H-13 and H-14 to C-3, C-4, and C-5, and from H-9 and H-10 to C-7 and C-8 as well as a H-10′ ↔ H-7 ↔ H-8 ↔ H-9/H-10 spin system seen in the ^{1}H–^{1}H COSY spectrum (see Fig. 3). Similarly, the presence of a 1,3,4-trisubstituted cyclohexane was supported by a H-5′↔H-6′↔H-1′↔H-2′↔H-3′ spin system observed in the ^{1}H–^{1}H COSY as well as by HMBC correlations from H-7′ to C-3′, C-4′, and C-5′ (Fig. 3). The downfield chemical shift of the quaternary carbon C-4′ (δ_C 71.6 ppm), the tertiary carbon C-3′ (δ_C 73.9 ppm) and H-3′ (δ_H 3.50 ppm) confirmed the presence of hydroxyl substituents at C-3′ and C-4′. The two substructures were connected through HMBC correlations from H-10′a to C-1′ and C-8′, and from H-10′b to C-6 and C-7. Although no HMBC correlations were observed over the C-5-O-C-8′ ether moiety, this ether linkage was confirmed based on ^{13}C NMR data, with C-8′ being downfield to the other possible positions, C-3′ and C-4′. Based on HMBC correlations to C-1′, C-8′, and C-10′, the unassigned methyl singlet (CH_3-9′) was positioned at the quaternary C-8′. The relative stereochemistry of the isobutyl syncarpic acid and cyclohexane moieties was determined through coupling constant analysis and

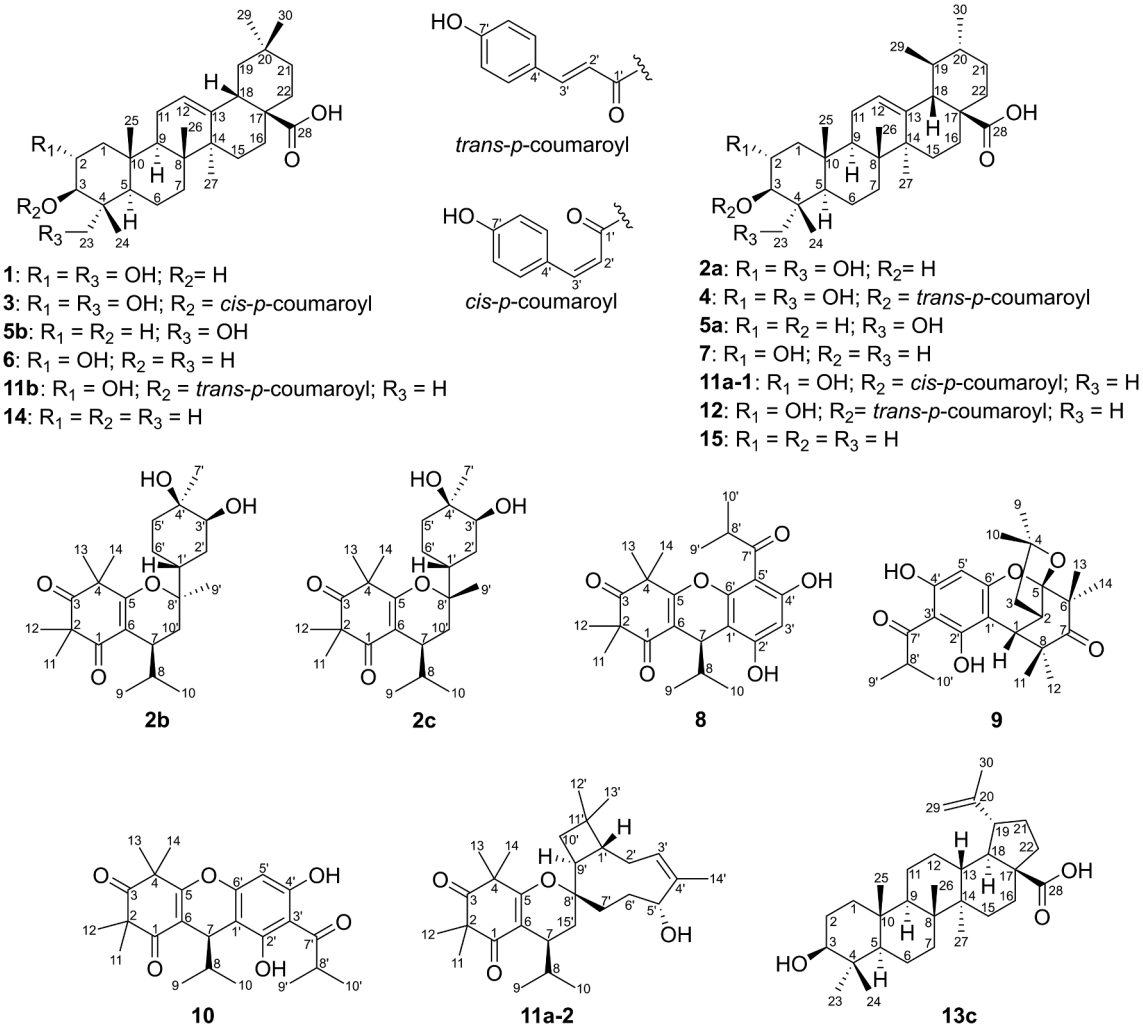

Fig. 2. Compounds identified from crude defatted chloroform leaves extract of *Myrtus communis*.

Table 1
IC_{50} values of *Myrtus communis* defatted chloroform extract, isolated compounds, and reference compounds RK-682 and acarbose against PTP1B and α-glucosidase.

Compound	Name	PTP1B[a,b]	α-glucosidase[a,b]
1	Arjunolic acid	34.82 ± 3.88	–
3	3β-*cis-p*-coumaroyloxy-2α,23-dihydroxyolean-12-en-28-oic acid	15.38 ± 0.87	–
4	3β-*trans-p*-coumaroyloxy-2α,24-dihydroxy-urs-12-en-28-oic acid	14.89 ± 0.36	–
5a	23-hydroxyursolic acid	56.38 ± 6.35	–
6	Maslinic acid	25.73 ± 0.82	> 100
7	Corosolic acid	12.21 ± 0.46	55.54 ± 3.14
8	Myrtucommulone B	39.71 ± 10.13	88.54 ± 16.28
9	5,7-dihydroxy-6-isobutyryl-2,2,10,10,12,12-hexamethyl- 2,3,3a,4-tetrahydro-4,9a-propanofuro[2,3-b]chromen-11-one	39.66 ± 4.56	85.79 ± 6.39
10	isomyrtucommulone B	8.93 ± 0.47	71.77 ± 9.05
11a-1	3β-*O-cis-p*-coumaroyl-2α-hydroxy-urs-12-en-28-oic acid	26.67 ± 0.35	–
11b	3β-*O-trans-p*-coumaroyl maslinic acid	69.39 ± 16.12	–
12	Jacoumaric acid	11.93 ± 0.31	> 100
13c	Betulinic acid	16.05 ± 1.34	> 100
14	Oleanolic acid	8.92 ± 0.46	34.29 ± 2.58
15	Ursolic acid	14.93 ± 0.58	62.27 ± 3.79
Chloroform extract		9.36 ± 0.54[c]	22.33 ± 1.23[c]
Reference compound	Acarbose	–	835.92 ± 30.85
	RK-682	7.35 ± 0.13	–

[a] IC_{50} values presented as mean value ± standard error (n = 3).
[b] μM.
[c] μg/mL.

Table 2
^{1}H and ^{13}C NMR data of **2b, 2c** and **11a-2** in methanol-d_4 (δ in ppm, J in Hz). [a]

	2b		**2c**		**11a-2**	
Pos.	δ_H, mult (J)	δ_C [b]	δ_H, mult (J)	δ_C [b]	δ_H, mult (J)	δ_C [b]
1	–	199.4	–	199.4	–	199.2
2	–	56.1	–	56.1	–	55.7
3	–	214.7	–	214.6	–	214.3
4	–	49.5	–	49.4	–	49.0
5	–	173.0	–	172.5	–	173.4
6	–	112.8	–	112.8	–	113.1
7	2.60, ddd (12.0, 6.5, 4.0)	33.7	2.72, ddd (12.0, 6.5, 4.0)	33.1	2.90, ddd (12.5, 7.7, 4.8)	34.1
8	2.70, m	27.0	2.70, m	26.8	2.19, m*	30.2
9	0.96, d (6.8)	20.7	0.98, d (6.8)	20.7	0.96, d (6.8)	20.7
10	0.64, d (6.8)	15.7	0.64, d (6.8)	15.7	0.74, d (6.8)	16.6
11	1.31, s	24.6	1.30, s	24.2	1.27, s	24.3
12	1.26, s	25.2	1.27, s	25.6	1.26, s	25.0
13	1.39, s	25.5	1.40, s	25.0	1.36, s	25.1
14	1.41, s	26.6	1.36, s	26.4	1.37, s	25.1
1′	2.07, tt(12.4,3.2)	33.9,	2.06, tt(12.4,3.2)	34.2	1.88, m*	47.9
2′a	1.67, m*	30.0	1.53, m*	31.4	2.16, m*	27.0
2′b	1.87, td(13.0,2.6)		1.71, td(13.0,2.6)		2.19, m*	
3′	3.50, brs	73.9	3.53, brs	74.0	5.47, t (8.4)	125.2
4′	–	71.6	–	71.6	–	140.2
5′a	1.52, m*	34.3	1.47, m*	33.8	4.27, dd (9.9, 3.6)	73.1
5′b	1.64, m*		1.52, m*			
6′a	1.38, m*	23.4	1.52, m*	22.0	1.84, m*	30.4
6′b	1.41, m*		1.61, m*		2.06, m	
7′a	1.16, s	27.5	1.16, s	27.5	1.70, m*	39.4
7′b	–		–		1.97,ddd (15.0, 10.4, 4.8)	
8′	–	83.5	–	83.5	–	84.5
9′	1.32, s	22.5	1.32, s	22.5	2.53, dt (10.4, 9.4)	43.8
10′a	1.48, m*	31.0	1.47, m*	30.8	1.44, dd (10.6, 8.4)	37.5
10′b	2.04, dd (14.4, 6.7)		2.02, dd (14.4, 6.7)		1.63, t (10.6)	
11′		–		–	–	35.6
12′		–		–	0.99, s	23.2
13′		–		–	0.98, s	30.0
14′		–		–	1.80, s	20.8
15′a		–		–	1.70, m*	29.4
15′b					2.18, m*	

*Multiplicities undetermined due to overlapping signals.
[a] Acquired at 600 MHz.
[b] ^{13}C NMR data were obtained from HSQC and HMBC spectra.

ROESY correlations. A ROE correlation between H-3′ and H-7′ showed these to be on the same side, i.e. pointing down according to Fig. 4, and the lack of a ROE between the 1,3-diaxial positioned H-1′ and H-3′ showed these to be on opposite sites. A triplet of doublets with coupling constant of 13.0 and 2.6 Hz, respectively, of H-2′b revealed this to be in an axial position with a geminal, an axial-axial, and an axial-equatorial coupling. H-3′ was shown as a broad singlet, consisting with an equatorial-axial coupling, putting H-1′ in an axial position, as shown in Fig. 4. A coupling constant of 12.0 Hz of H-7 indicated this to be in an axial position, in accordance with myrtucommulone L at the same position (Cottiglia et al., 2012). Furthermore, the lack of correlation between the pseudo 1,3-diaxial positioned H-7 and H-1′ showed that the cyclohexane moiety is on the opposite side of H-7 (see Fig. 4). This was further supported by the ROE correlations between H-7 and H-10′b as well as H-10′b and H-9′, positioning H-9′ on the same side as H-7. Thus, the structure of **2b** was elucidated as shown in Fig. 2 and named *rel*-(2S,4R)-2-((1R,3S,4R)-3,4-dihydroxy-4-methylcyclohexyl)-4-isopropyl-2,6,6,8,8-pentamethyl-2,3,4,8-tetrahydro-5*H*-chromene-5,7(6*H*)-dione. However, due to the lack of ROE correlations between the two structural moieties, the stereochemistry of the cyclohexane, relative to the isobutyl syncarpic acid, could be inverted. All 1D and 2D NMR spectra are given in Supplementary Figs. S3–S7. The absolute configuration was sought elucidated through a Mosher ester analysis, but due to the limited amount, this proved unsuccessful.

Compound **2c** was obtained as a white gum. The assignment of its molecular formula as $C_{24}H_{38}O_5$ was based on the quasi-molecular ion observed in the HRESI(+)MS spectrum at m/z 407.2788 $[M + H]^+$ (calcd for $C_{24}H_{39}O_5^+$ 407.2792, ΔM 1.0 ppm). The HMBC and COSY spectroscopic data analysis revealed **2b** and **2c** to be structurally similar with the most remarkable difference detected in chemical shift at chiral centre C-7 (δ_C 33.7 ppm, δ_H 2.60 ppm for **2b**; δ_C 33.1 ppm, δ_H 2.72 ppm for **2c**) (Table 2). With nearly identical coupling constants of H-7 for both compounds, epimerization at C-7 was discarded, indicating a spatial effect in consequence of different orientation of the cyclohexane at C-8′. This was further confirmed by a ROESY correlation observed between the pseudo 1,3-diaxial positioned H-7 and H-1′ in **2c**, positioning the cyclohexane moiety on the same side as H-7 (see Fig. 4). This identified **2c** to be an epimer of **2b** at C-8′. Thus, the structure of **2c** was elucidated as shown in Fig. 2 and given the name *rel*-(2S,4S)-2-((1R,3S,4R)-3,4-dihydroxy-4-methylcyclohexyl)-4-isopropyl-2,6,6,8,8-pentamethyl-2,3,4,8-tetrahydro-5*H*-chromene-5,7(6*H*)-dione. Similar to **2b**, the stereochemistry of the cyclohexane, relative to the isobutyl syncarpic acid moiety, could be inverted. All 1D and 2D NMR spectra are given in Supplementary Figs. S8–S12. The absolute configuration was sought elucidated through a Mosher ester analysis, but due to the limited amount, this proved unsuccessful.

Compound **11a-2** was obtained as a white gum. The assignment of its molecular formula as $C_{29}H_{44}O_4$ was based on the quasi-molecular ion observed in the HRESI(+)MS at m/z 457.3327 $[M + H]^+$ (calcd for $C_{29}H_{45}O_4^+$ 457.3312, ΔM −3.2 ppm). The ^{1}H NMR data of **11a-2** indicated the presence of an oxymethine proton at δ 4.27 ppm (dd, J = 9.9, 3.6 Hz, H-5′), an olefinic proton at δ 5.47 ppm (t, J = 8.4 Hz, H-3′), two methyl doublets at δ 0.96 ppm (J = 6.8 Hz, CH_3-9) and 0.74 ppm (J = 6.8 Hz, CH_3-10), and seven methyl singlets at δ 1.80 ppm

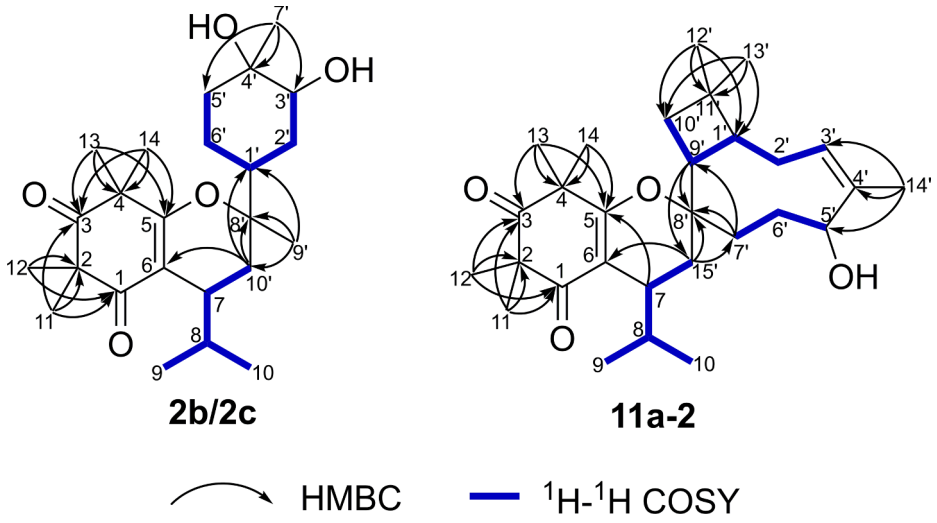

Fig. 3. Selected HMBC and ^{1}H–^{1}H COSY correlations of **2b**, **2c**, and **11a-2**.

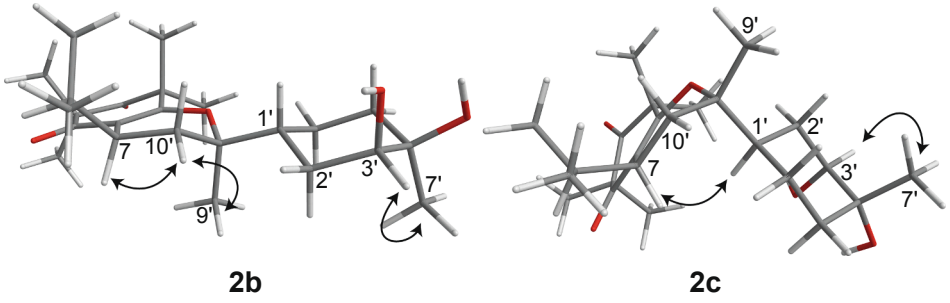

Fig. 4. Key ROE correlations of **2b** and **2c**.

(CH_3-14′), 1.37 ppm (CH_3-14), 1.36 ppm (CH_3-13), 1.27 ppm (CH_3-11), 1.26 ppm (CH_3-12), 0.99 ppm (CH_3-12′), and 0.98 ppm (CH_3-13′) (Table 2). ^{13}C NMR chemical shift values obtained from HSQC and HMBC spectra indicated the presence of 29 carbons, which included nine methyl carbons at δ 30.0 ppm, 25.1 ppm, 25.1 ppm, 25.0 ppm, 24.3 ppm, 23.2 ppm, 20.8 ppm, 20.7 ppm, 16.6 ppm, two carbonyl carbons at δ 214.3 ppm and 199.2 ppm, four olefinic carbons at δ 173.4 ppm, 140.2 ppm, 125.2 ppm, and 113.1 ppm, and two oxygenated carbons at δ 84.5 ppm and 73.1 ppm (Table 2). Similar to **2b** and **2c**, an isobutyl syncarpic acid moiety was observed in compound **11a-2**. Furthermore, comparison of ^{1}H and ^{13}C chemical shifts of **11a-2** with known isomers, Tomentodione O and Tomentodione P (Zhang et al., 2018), suggested the presence of a caryophyllenyl alcohol moiety (Fig. 3). Similar to **2b** and **2c**, HMBC correlations from H-11 and H-12 to C-1, C-2, and C-3, from H-13 and H-14 to C-3, C-4, and C-5, from H-9 and H-10 to C-8, from H-8 to C-6, and from H-7 to C-5 (see Fig. 3), confirmed the isobutyl syncarpic acid moiety in **11a-2**. The caryophyllenyl alcohol moiety was confirmed by HMBC correlations from H-9′ to C-1′, C-2′, and C-8′, from H-7′a to C-5′, C-8′, and C-9′, from H-12′ and H-13′ to C-1′, C-10′, and C-11′, and from H-14′ to C-3′, C-4′, and C-5′ as well as H-3′ ↔ H-2′ ↔ H-1′ ↔ H-9′ ↔ H-10′ and H-5′ ↔ H-6′ ↔ H-7′ spin systems observed in the ^{1}H-^{1}H COSY spectrum (see Fig. 3). The spiro junction between the isobutyl syncarpic acid and caryophyllenyl alcohol moieties was established based on the HMBC correlations from H-15′a to C-7′, C-8′, and C-9′, from H-9′ to C-7′, C-8′, and C-15′, and from H-7′ to C-8′, C-9′, and C-15′ (Fig. 3). The relative configuration was determined through ROE correlations. A strong correlation between H-3′ and H-14′ in **11a-2** implied *Z* configuration of the olefinic bond between C-3′ and C-4′, which was in agreement with the configuration reported for the related compounds Tomentodione O and Tomentodione P (Zhang et al., 2018). The ROE observed between H-1′ and H-13′/H-5′ indicated these to be on the same side, arbitrarily designated as having α-configuration. Due to overlap between signals from H-15′a and H-7′a relative stereochemistry could not be determined directly by ROE correlations from H-8/H-9/H-11 as done for Tomentodione O and P. However, correlations between H-9′ and H-12′/H-7 together with the absence of correlations between H-9/H-10 and H-9′/H-10′a/b showed both H-7 and H-9′ to be in a β-configuration. The relative stereochemistry of **11a-2**, shown in Fig. 2, corresponds to Tomentodione O and was further supported by similar chemical shifts and coupling constants. The new compound, **11a-2**, was given the trivial name myrtucommulone Q. All 1D and 2D NMR spectra are given in Supplementary Figs. S20–S24.

4. Conclusions

In this study, the potential of *M. communis* as a bifunctional food for treatment of T2D was evaluated by investigation of individual PTP1B and α-glucosidase inhibitors from the chloroform extract of *M. communis* leaves. Dual high-resolution PTP1B and α-glucosidase profiling in combination with analytical-scale HPLC separation led to identification of 14 active triterpenoids and three active phloroglucinol derivatives. In addition, three previously undescribed phloroglucinol derivatives were identified. These results support the potential of *M. communis* as a bifunctional food for treatment of T2D.

Ethic statement

Our research did not include any human subjects and animal experiments.

Declaration of Competing Interest

The authors declare no conflicts of interest.

Acknowledgements

The analytical scale HPLC used for high-resolution inhibition profiling and isolation of compounds was obtained via a grant from The Carlsberg Foundation. The HPLC-HRMS and NMR equipment were acquired through a grant from “Apotekerfonden af 1991”, The Carlsberg Foundation, and the Danish Agency for Science, Technology and Innovation via the National Research Infrastructure funds. C.L. acknowledges the Chinese Scholarship Council for a PhD scholarship (CSC No. 201608610129). Arife Önder is thanked for technical assistance.

Appendix A. Supplementary material

Supplementary data to this article can be found online at https://doi.org/10.1016/j.jff.2019.103623.

References

Aguirre, M. C., Delporte, C., Backhouse, N., Erazo, S., Letelier, M. E., Cassels, B. K., ... Negrete, R. (2006). Topical anti-inflammatory activity of 2α-hydroxy pentacyclic triterpene acids from the leaves of *Ugni molinae*. *Bioorganic & Medicinal Chemistry, 14*, 5673–5677.

Alipour, G., Dashti, S., & Hosseinzadeh, H. (2014). Review of pharmacological effects of *Myrtus communis* L. and its active constituents. *Phytotherapy Research, 28*, 1125–1136.

American Diabetes Association (2013). Diagnosis and classification of diabetes mellitus. *Diabetes Care, 36*, S67–S74.

Appendino, G., Bianchi, F., Minassi, A., Sterner, O., Ballero, M., & Gibbons, S. (2002). Oligomeric acylphloroglucinols from Myrtle (*Myrtus communis*). *Journal of Natural Products, 65*, 334–338.

Appendino, G., Maxia, L., Bettoni, P., Locatelli, M., Valdivia, C., Ballero, M., ... Sterner, Olov (2006). Antibacterial galloylated alkylphloroglucinol glucosides from Myrtle (*Myrtus communis*). *Journal of Natural Products, 69*, 251–254.

Bokor, É., Kun, S., Goyard, D., Tóth, M., Praly, J.-P., Vidal, S., & Somsák, L. (2017). C-glycopyranosyl arenes and hetarenes: Synthetic methods and bioactivity focused on antidiabetic potential. *Chemical Reviews, 117*, 1687–1764.

Chalchat, J.-C., Garry, R.-P., & Michet, A. (1998). Essential oils of myrtle (*Myrtus communis* L.) of the mediterranean littoral. *Journal of Essential Oil Research, 10*, 613–617.

Chen, M., Chen, L.-F., Li, M.-M., Li, N.-P., Cao, J.-Q., Wang, Y., ... Ye, W.-C. (2017). Myrtucomvalones A-C, three unusual triketone–sesquiterpene adducts from the leaves of *Myrtus communis* ‘Variegata’†. *RSC Advances, 7*, 22735–22740.

Choudhary, M. I., Khan, N., Ahmad, M., Yousuf, S., Fun, H.-K., Soomro, S., ... Shaheen, F. (2013). New inhibitors of ROS generation and T-Cell proliferation from *Myrtus communis*. *Organic Letters, 15*, 1862–1865.

Cottiglia, F., Casu, L., Leonti, M., Caboni, P., Floris, C., Busonera, B., ... Sanna, G. (2012). Cytotoxic phloroglucinols from the leaves of *Myrtus communis*. *Journal of Natural Products, 75*, 225–229.

Eyong, K. O., Bairy, G., Eno, A. A., Taube, J., Hull, K. G., Folefoc, G. N., ... Romo, D. (2018). Triterpenoids from the stem bark of *Vitellaria paradoxa* (Sapotaceae) and derived esters exhibit cytotoxicity against a breast cancer cell line. *Medicinal Chemistry Research, 27*, 268–277.

Fang, L., Cao, J., Duan, L., Tang, Y., & Zhao, Y. (2014). Protein tyrosine phosphatase 1B (PTP1B) and α-glucosidase inhibitory activities of *Schisandra chinensis* (Turcz.) Baill. *Journal of Functional Foods, 9*, 264–270.

Funakoshi, M., Azami, Y., Matsumoto, H., Ikota, A., Ito, K., Okimoto, H., ... Miura, J. (2017). Socioeconomic status and type 2 diabetes complications among young adult patients in Japan. *PLoS ONE, 12* e0176087.

Gu, J.-Q., Park, E. J., Luyengi, L., Hawthorne, M. E., Mehta, R. G., Farnsworth, N. R., ... Kinghorn, A. D. (2001). Constituents of *Eugenia sandwicensis* with potential cancer chemopreventive activity. *Phytochemistry, 58*, 121–127.

Häberlein, H., & Tschiersch, K.-P. (1994). Triterpenoids and flavonoids from *Leptospermum scoparium*. *Phytochemistry, 35*, 765–768.

Hu, P., Li, D.-H., Jia, C.-C., Liu, Q., Wang, X.-F., ... Hua, H.-M. (2017). Bioactive constituents from *Vitex negundo* var. *heterophylla* and their antioxidant and α-glucosidase inhibitory activities. *Journal of Functional Foods, 35*, 236–244.

Huang, X., Yi, W., Yi, L., Bie, Q., & Peng, S. (2015). Research advances for hot targets of diabetes treatment. *Zhongguo Xinyao Zazhi, 24*, 526–532 (in Chinese).

Ibrahim, M. A., Bester, M. J., Neitz, A. W. H., & Gaspar, A. R. M. (2018). Structural properties of bioactive peptides with α-glucosidase inhibitory activity. *Chemical Biology & Drug Design, 91*, 370–379.

International diabetes federation. IDF Diabetes Atlas, 8th ed., 2015, ISBN 978-2-930229-87-4. http://www.diabetesatlas.org/ (accessed on 09/04/2018).

Jaiswal, N., Srivastava, S. P., Bhatia, V., Mishra, A., Sonkar, A. K., Narender, T., ... Tamrakar, A. K. (2012). Inhibition of alpha-glucosidase by *Acacia nilotica* prevents hyperglycemia along with improvement of diabetic complications via aldose reductase inhibition. *Journal of Diabetes and Metabolism* S:6.

Johnson, T. O., Ermolieff, J., & Jirousek, M. R. (2002). Protein tyrosine phosphatase 1B inhibitors for diabetes. *Nature Reviews Drug Discovery, 1*, 696–709.

Kazmi, M., Zaib, S., Ibrar, A., Amjad, S. T., Shafique, Z., Mehsud, S., ... Khan, I. (2018). A new entry into the portfolio of α-glucosidase inhibitors as potent therapeutics for type 2 diabetes: Design, bioevaluation and one-pot multi-component synthesis of diamine-bridged coumarinyl oxadiazole conjugates. *Bioorganic Chemistry, 77*, 190–202.

Kongstad, K. T., Özdemir, C., Barzak, A., Wubshet, S. G., & Staerk, D. (2015). Combined use of high-resolution α-glucosidase inhibition profiling and HPLC-HRMS-SPE-NMR for investigation of antidiabetic principles in crude plant extracts. *Journal of Agricultural and Food Chemistry, 63*, 2257–2263.

Lee, T.-H., Juang, S.-H., Hsu, F.-L., & Wu, C.-Y. (2005). Triterpene acids from the leaves of *Planchonella duclitan* (Blanco) Bakhuizan. *Journal of the Chinese Chemical Society, 52*, 1275–1280.

Lima, R. C. L., Kato, L., Kongstad, K. T., & Staerk, D. (2018). Brazilian insulin plant as a bifunctional food: Dual high-resolution PTP1B and α-glucosidase inhibition profiling combined with HPLC-HRMS-SPE-NMR for identification of antidiabetic compounds in *Myrcia rubella* Cambess. *Journal of Functional Foods, 45*, 444–451.

Lima, R. C. L., Kongstad, K. T., Kato, L., Silva, M. J., Franzyk, H., & Staerk, D. (2018). High-resolution PTP1B inhibition profiling combined with HPLC-HRMS-SPE-NMR for identification of PTP1B inhibitors from *Miconia albicans*. *Molecules, 23*, 1755–1767.

Liu, C., Ang, S., Huang, X.-J., Tian, H.-Y., Deng, Y.-Y., Zhang, D.-M., ... Wang, L. (2016). Meroterpenoids with new skeletons from *Myrtus communis* and structure revision of myrtucommulone K. *Organic Letters, 18*, 4004–4007.

Liu, H., Huo, L., Yang, B., Yuan, Y., Zhang, W., Xu, Z., ... Tan, H. (2017). Biomimetic-inspired syntheses of myrtucommuacetalone and myrtucommulone. *J. Organic Letters, 19* 4786–4089.

Liu, B., Kongstad, K. T., Wiese, S., Jäger, A. K., & Staerk, D. (2016). Edible seaweed as future functional food: Identification of α-glucosidase inhibitors by combined use of high-resolution α-glucosidase inhibition profiling and HPLC–HRMS–SPE–NMR. *Food Chemistry, 203*, 16–22.

Lv, L., Li, Y., Zhang, Y., & Xie, Z. (2017). Biomimetic synthesis of myrtucommulone K, N and O. *Tetrahedron, 73*, 3691–3695.

Malekpour, A., Dehghani, S., Zahedi, S., & Eskandari, F. (2012). Effects of the hydro-ethanol extract of *Myrtus communis* L. on blood glucose level and histopathological changes in alloxan-induced diabetic rats. *Middle-East Journal of Scientific Research, 12*, 517–522.

Martinez, A., Rivas, F., Perojil, A., Parra, A., Garcia-Granados, A., & Fernandez-Vivas, A. (2013). Biotransformation of oleanolic and maslinic acids by *Rhizomucor miehei*. *Phytochemistry, 94*, 229–237.

Önal, S., Timur, S., Okutucu, B., & Zihnioğlu, F. (2005). Inhibition of α-glucosidase by aqueous extracts of some potent antidiabetic medicinal herbs. *Preparative Biochemistry and Biotechnology, 35*, 29–36.

Rosa, A., Deiana, M., Casu, V., Corona, G., Appendino, G., Bianchi, F., ... Dessi, M. A. (2003). Antioxidant activity of oligomeric acylphloroglucinols from *Myrtus communis* L. *Free Radical Research, 37*, 1013–1019.

Ryu, H. W., Cho, J. K., Curtis-Long, M. J., Yuk, H. J., Kim, Y. S., Jung, S., ... Park, K. H. (2011). α-Glucosidase inhibition and antihyperglycemic activity of prenylated xanthones from *Garcinia mangostana*. *Phytochemistry, 72*, 2148–2154.

Sashida, Y., Ogawa, K., Yamanouchi, T., Tanaka, H., Shoyama, Y., & Nishioka, I. (1994). Triterpenoids from callus tissue of *Actznzdza polygama*. *Phytochemistry, 35*, 377–380.

Schmidt, J. S., Lauridsen, M. B., Dragsted, L. O., Nielsen, J., & Staerk, D. (2012). Development of a bioassay-coupled HPLC-SPE-ttNMR platform for identification of α-glucosidase inhibitors in apple peel (Malus × domestica Borkh.). *Food Chemistry, 135*, 1692–1699.

Schmidt, J. S., Nyberg, N. T., & Staerk, D. (2014). Assessment of constituents in *Allium* by multivariate data analysis, high-resolution α-glucosidase inhibition assay and HPLC-SPE-NMR. *Food Chemistry, 161*, 192–198.

Seitimova, G. A., Eskalieva, B. K., Burasheva, G. S., & Choudhary, M. I. (2018). Phenanthrenes from *Kochia prostrata*. *Chemistry of Natural Compounds, 54*, 749–750.

Shaheen, F., Ahmad, M., Khan, S. N., Hussain, S. S., Anjum, S., Tashkhodjaev, B., ... Rahman, A. (2006). New α-glucosidase inhibitors and antibacterial compounds from *Myrtus communis* L. *European Journal of Organic Chemistry, 10*, 2371–2377.

Sisay, M., & Gashaw, T. (2017). Ethnobotanical, ethnopharmacological, and phytochemical studies of *Myrtus communis* Linn: A popular herb in Unani system of medicine. *Journal of Evidence-Based Complementary & Alternative Medicine, 22*, 1035–1043.

Tamrakar, A. K., Maurya, C. K., & Rai, A. K. (2014). PTP1B inhibitors for type 2 diabetes treatment: A patent review. (2011–2014). *Expert Opinion on Therapeutic Patents, 24*, 1101–1115.

Tryggestad, J. B., & Willi, S. M. (2015). Complications and comorbidities of T2DM in adolescents: Findings from the TODAY clinical trial. *Journal of Diabetes and Its Complications, 29*, 307–312.

Wang, Y., Xiang, L., Chen, M., Zhang, Z., & He, X. (2012). Substrate specificity for the 2α-hydroxylation of ursolic acid by *Alternaria alternata* and the antitumor activities of those metabolites. *Journal of Molecular Catalysis B: Enzymatic, 83*, 51–56.

Wiechmann, K., Müller, H., Huch, V., Hartmann, D., Werz, O., & Jauch, J. (2015). Synthesis and biological evaluation of novel myrtucommulones and structural analogues that target mPGES-1 and 5-lipoxygenase. *European Journal of Medicinal Chemistry, 101*, 133–149.

Wubshet, S. G., Tahtah, Y., Heskes, A. M., Kongstad, K. T., Pateraki, I., Hamberger, B., ... Staerk, D. (2016). Identification of PTP1B and α-glucosidase inhibitory Serrulatanes from *Eremophila spp.* by combined use of dual high-resolution PTP1B and α-glucosidase inhibition profiling and HPLC-HRMS-SPE-NMR. *Journal of Natural Products, 79*, 1063–1072.

Xiao, T., Guo, Z., Sun, B., & Zhao, Y. (2017). Identification of anthocyanins from four kinds of berries and their inhibition activity to α-glycosidase and protein tyrosine phosphatase 1B by HPLC－FT-ICR MS/MS. *Journal of Agricultural and Food Chemistry,*

65, 6211–6221.
Yue, J., Xu, J., Cao, J., Zhang, X., & Zhao, Y. (2017). Cucurbitane triterpenoids from *Momordica charantia* L. and their inhibitory activity against α-glucosidase, α-amylase and protein tyrosine phosphatase 1B (PTP1B). *Journal of Functional Foods, 37*, 624–631.
Zabolotny, J. M., Kim, Y. B., Welsh, L. A., Kershaw, E. E., Neel, B. G., & Kahn, B. B. (2008). Protein-tyrosine phosphatase 1B expression is induced by inflammation in vivo. *Journal of Biological Chemistry, 283*, 14230–14241.
Zebiri, I., Haddad, M., Duca, L., Sauvain, M., Paloque, L., Cabanillas, B., ... Voutquenne-Nazabadiokoa, L. (2017). Biological activities of triterpenoids from *Poraqueiba sericea* stems. *Natural Product Research, 31*, 1333–1338.
Zhang, Y.-B., Li, W., Jiang, L., Yang, L., Chen, N.-H., Wu, Z.-N., ... Wang, G.-C. (2018). Cytotoxic and anti-inflammatory active phloroglucinol derivatives from *Rhodomyrtus tomentosa*. *Phytochemistry, 153*, 111–119.
Zhao, Y., Chen, M. X., Kongstad, K. T., Jäger, A. K., & Staerk, D. (2017). Potential of *Polygonum cuspidatum* root as an antidiabetic food: Dual high-Resolution α-glucosidase and PTP1B inhibition profiling combined with HPLC-HRMS and NMR for identification of antidiabetic constituents. *Journal of Agricultural and Food Chemistry, 65*, 4421–4427.
Zhao, Y., Kongstad, K. T., Jäger, A. K., Nielsen, J., & Staerk, D. (2018). Quadruple high-resolution α-glucosidase/α-amylase/PTP1B/radical scavenging profiling combined with high-performance liquid chromatography-high-resolution mass spectrometry-solid-phase extraction-nuclear magnetic resonance spectroscopy for identification of antidiabetic constituents in crude root bark of *Morusalba* L. *Journal of Chromatography A, 1556*, 55–63.
Zhao, Y., Kongstad, K. T., Liu, Y., He, C., & Staerk, D. (2019). Unraveling the complexity of complex mixtures by combining high-resolution pharmacological, analytical and spectroscopic techniques: Antidiabetic constituents in Chinese medicinal plants. *Faraday Discussions, 218*, 202–218.
Zhao, T. B., Nguyen, D. H., Le, D. D., Choi, J. S., Min, B. S., & Woo, M. H. (2018). Protein tyrosine phosphatase 1B inhibitors from natural sources. *Archives of Pharmacal Research, 41*, 130–161.